

Electron Energy Conversion to EUV Radiation in the K_α Line of Be in the “Shooting Through” Geometry

A. Ya. Lopatin^a, D. E. Par'ev^a, A. E. Pestov^{a,*}, N. N. Salashchenko^a, N. I. Chkhalo^a,
G.H. N. Demin^b, N. A. Dyuzhev^b, M. A. Makhaboroda^b, and A. A. Kochetkov^c

^a Institute of Physics of Microstructures, Russian Academy of Sciences, Nizhny Novgorod, 603950 Russia

^b MIET National Research University, Zelenograd, Moscow, 124498 Russia

^c Lobachevskii Nizhny Novgorod State University, Nizhny Novgorod, 603950 Russia

*e-mail: aepestov@ipm.sci-nnov.ru

Received March 30, 2018

Abstract—A model is presented and the interaction of accelerated electrons with atoms in a thin film “shooting through” a Be target is theoretically described. The algorithm is based on the Monte Carlo simulation of the electron motion in the target accompanied by energy losses in elastic and inelastic interactions. The conversion of the electron energy to the radiation energy in the 11.4-nm K_α line of Be and the emission spectrum are calculated. The maximum conversion efficiency to the solid angle 4π $CE = 3.0 \times 10^{-4}$ is achieved for the electron energy $E_e = 2.0$ keV and a 40 nm thick freely suspended beryllium film. 200 nm and 400 nm thick films were experimentally investigated. The maximum conversion efficiency to the solid angle 4π for a 200 nm thick film and the electron energy $E_e = 2.75$ keV was $CE_{\text{exp}} = 9.2 \times 10^{-5}$, whereas the calculated value was $CE_{\text{calc}} = 2.5 \times 10^{-4}$. The observed discrepancy between the theory and experiment is explained in the paper.

DOI: 10.1134/S1063776118100175

1. INTRODUCTION

In [1], a new scheme of a projection lithograph for extremal UV (EUV) radiation and soft X-rays is proposed, which significantly simplifies and reduces the cost of the lithographic process and the lithograph itself. This scheme differs from a classical projection lithograph in that it combines the functions of a mask and a EUV radiation source in one element—an array of microfocus X-ray tubes. The idea is based on using the technology of autoemission silicon nanocathodes—triodes with a rather high mean current density (up to 1 A/cm²) developed by now [2]. By controlling each individual cathode, it is possible to control with high frequency an electron microbeam current. By placing a thin film nearby and applying to it the appropriate potential difference, we can generate X-rays upon absorption of the electron beam in the film; i.e., we will have an X-ray source array with small pixels. By controlling the states of individual pixels, it is possible to form the topology of the source, thereby having an analog of a conventional mask for projection lithography, but a dynamic mask with a changeable topology. An objective transfers a diminished source image on a semiconductor plate with a photoresist, the displacements of the plate during exposure being syn-

chronized with the switching of pixels in the microfocus tube array.

An important parameter of the lithographic process is the exposure rate, which is directly proportional to the X-ray radiation power incident on the plate P_x with a photoresist and can be written in the form

$$P_x = P_e CE \frac{\Omega_{\text{in}}}{4\pi} R_m^2, \quad (1)$$

where CE is the conversion efficiency (conversion coefficient) of the electron energy P_e into the X-ray line energy emitted with 4π steradian; Ω_{in} is the solid angle within which the source radiation falls to the objective (the useful source radiation); and R_m is the reflection coefficient of mirrors of a projection two-mirror objective considered in [1].

According to [3], the 11.4-nm K_α line of beryllium seems the most promising for this problem. The reflection coefficient of multilayer X-ray Mo/Be mirrors in this spectral range amounts to $R_m = 0.7$ [4]. By substituting to (1) the parameters of the objective and the chip of microfocus tubes from [1] and estimating the conversion efficiency of the electron energy to the Be K_α line radiation by the probability of the radiative decay of the excited atom taken from [5], the expected output of the lithographic process for the typical sen-

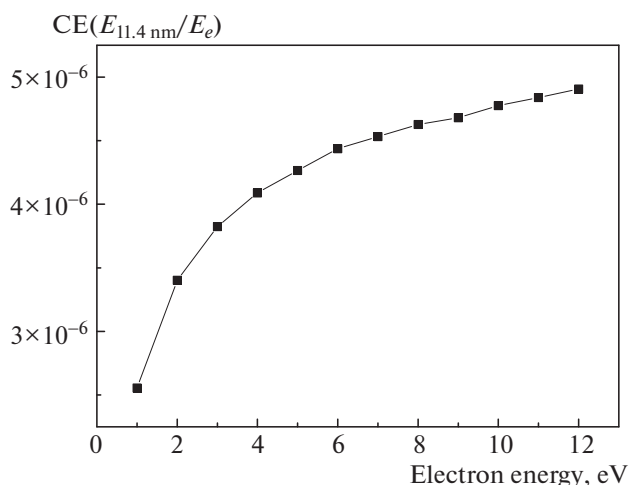


Fig. 1. Dependence of the conversion coefficient of the electron energy to the energy of the characteristic Be K_{α} line on the incident electron energy obtained using the WinXray software [9].

sitivity of photoresists in this range about 10 mJ/cm^2 will be $1.10 \times 10^{-2} \text{ cm}^2/\text{s}$ or about 0.5 plate 100 mm in diameter per hour. Note that this exposure rate is provided during the formation of nanostructures with the minimal technological size $hp = 20 \text{ nm}$ (half-pitch), it exceeds by approximately three orders of magnitude the efficiency of a single-beam electron lithograph and is quite sufficient for small and even medium-size microcircuit production.

The coefficient CE is determined by the ionization efficiency of the electron shell and the probability of the radiative decay of the excited state of the ion upon filling of the produced hole by an electron from the upper shell, and its value is unknown. The goals of this study are to estimate the radiation efficiency of an X-ray tube with a beryllium target in the “shooting through” geometry and to determine the CE of the electron energy to the energy of the characteristic Br K_{α} line. The results of Monte Carlo simulations and experimental measurements of the emission of a thin film Be target are presented.

2. MONTE CARLO SIMULATIONS

The generation of radiation in an X-ray tube is a probabilistic process that can be described by Monte Carlo simulations of the interaction of electrons with target atoms. At present, a great number of software packages are available on the Internet [6–8] for calculating fluorescence line intensities, the electron penetration depth, and the absorption depth. However, all these programs either have no data on the spectral lines of light elements, including the K_{α} line of Be, or perform calculations based on semi-empirical interaction cross sections whose reliability is confirmed only for nuclear charges $Z > 6$. Moreover, calculations are

performed for the “reflection” geometry; i.e., the reflection of radiation to the same half-space from which electrons are incident is considered.

Figure 1 demonstrates the dependence of the electron energy CE to the energy of the Be characteristic K_{α} line on the incident electron energy calculated with the help of the WinXray software using ionization cross sections from [9]. The absolute conversion efficiency is defined as the ratio of the energy of the Be K_{α} line emitted into the solid angle 4π to the electron beam energy.

One can see that the CE increases in the entire electron energy range up to 12 keV, which contradicts the data from [10], where the radiation intensity increases up to the electron energy about 10 ionization potentials. Then, the radiation intensity begins to decrease noticeably with increasing the electron energy, because of electron scattering in the target and radiation self-absorption. The ionization potential for the beryllium K level is $E_i = 111.5 \text{ eV}$ [11].

The CE value was only 4.9×10^{-6} . This casts serious doubts, because the emission probability of the Be K_{α} line is $\omega_K = 3.6 \times 10^{-4}$ [5], and due to weak scattering of electrons by light element atoms, the total cross section for elastic scattering should not exceed the cross section for inelastic scattering more than two orders of magnitude. Moreover, it was stated in [9] that the model is valid for $6 < Z < 79$. Thus, the model used in the WinXray software for calculating the absolute radiation intensity of solid targets cannot be considered correct and, therefore, it is necessary to perform alternative simulations based on more adequate interaction cross sections.

We used the model described in [12] and beryllium ionization cross sections from [13]. Figure 2 presents ionization cross sections for the Be K level calculated by models [9] and [13].

One can see that the cross section from [13] has a maximum in the vicinity of 100 eV (near the K edge of Be), which suggests that this model is more adequate than that used in the WinXray software [9].

The general calculation scheme includes the following steps:

The drawing of the process type (elastic or inelastic scattering),

the drawing of the lost energy value,

the drawing of the azimuthal angle,

the drawing of the mean free path.

Such a model allows one to study the behavior of the electron beam and target by fixing at each step the energy, the motion direction, the depth under the surface, and other parameters of interest.

The process type is determined from the distribution $P_i = \sigma_i/(\sigma_i + \sigma_e)$; $P_e = 1 - P_i$. Here, σ_i and σ_e are the integrated cross sections for inelastic and elastic interactions, respectively.

The cross section σ_e is calculated from the expression [14]

$$\sigma_e(E) = \frac{16m^2 Z^4 e^4 \phi^4 \pi}{\hbar^4 (8mE\phi^2 \hbar^{-2} + 1)}, \quad (2)$$

where $\phi = 0.855a_0 Z^{-1/3}$ is the screening radius, a_0 is the radius of the first Bohr orbital, Z is the nucleus charge, m is the electron mass, e is the electron charge, and E is the incident electron energy.

The total cross section for inelastic scattering is obtained from the Bethe formula [15]

$$\sigma_i(E) = \frac{2\pi e^4 Z}{JE} \ln\left(\frac{1.166E}{J}\right), \quad (3)$$

where J is the mean excitation potential of the atom. It follows from the Bloch theory [16] based on the statistical Thomas–Fermi atomic model that $J = kZ$, where $k \approx 13.5$ eV.

The cosine of the azimuthal angle is calculated from the formula

$$\cos \varphi = \cos(2\pi\gamma), \quad (4)$$

where γ is a random number in the interval $[0, 1]$, assuming that any angle φ is equiprobable.

A new value of the angle with respect to the normal to the surface after the l th collision is defined as

$$\cos \beta_l = \cos \beta_{l-1} \cos \theta_l + \sin \beta_{l-1} \sin \theta_l \cos \varphi_l, \quad (5)$$

where β is the angle with respect to the normal to the surface and θ is the polar angle.

The drawing of the mean free path λ_l is performed and the depth D of next collision is calculated by the formula

$$D = D + \lambda_l \cos \beta_l. \quad (6)$$

The condition of the electron backscattering or escape from the target ($0 < D < d$, d is the film thickness) is verified.

The characteristic line intensity is calculated as follows.

(1) The ionization and excitation cross sections are determined for all possible transitions. The ionization cross section for an individual level is taken from [13]:

$$\sigma_q(t) = \frac{S}{t+u+1} \left[\frac{\ln(t)}{2} \left(1 + \frac{1}{t^2}\right) + 1 - \frac{1}{t} - \frac{\ln(t)}{t+1} \right], \quad (7)$$

$$S = \frac{4\pi a_0^2 N R^2}{B_q}, \quad (8)$$

where N is the number of orbital electrons, $t = E/B_q$, $u = U/B_q$, R is the Rydberg constant, $U = \langle p^2/2m \rangle$ is the orbital kinetic energy, and B_q is the bond energy of the q th level. The excitation cross section was determined by the scaling method [17] from the expression

$$\sigma_{ex} = \frac{\sigma_q E}{E + B_q + C_q}, \quad (9)$$

Ionization cross section, cm^2

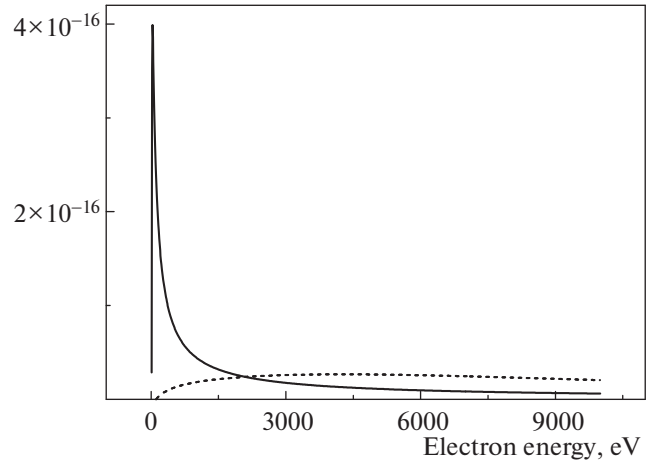


Fig. 2. Dependences of the ionization cross section for the K shell of a beryllium atom on the incident electron energy plotted by data from [9] (dashed curve) and [123] (solid curve).

where C_q is the excitation energy of the q th level.

The line intensities were calculated using probabilities presented in [5].

(2) Taking into account data on the probabilities of the fluorescence and Auger process yield [5] and transition energies [18], the amount of photons emitted by the given atom in the given line is determined.

(3) Taking into account the photon creation depth, its energy, and the permittivity corresponding to this energy [19], the number of photons escaped from the target is determined.

This model was used for calculating the radiation intensity of a beryllium target in the shooting through geometry (within a solid angle of 4π) as a function of the incident electron energy (the angle of incidence of electrons on the target was assumed zero in all calculations) and the Be film thickness. The CE of the electron energy to the characteristic Be 11.4-nm K_α line energy was calculated from these data. The energy range was from 0.5 to 10 keV. The electron current was taken to be 1.0 A in all calculations (corresponding to 6.25×10^{18} electrons per second). Figure 3 presents the typical emission spectrum of the beryllium target in the shooting through geometry. The calculation parameters were: the electron energy $E_e = 1.0$ keV, the angle of incidence $\theta_{in} = 0$, and the film thickness $d = 200$ nm.

One can see that the spectrum is a combination of the characteristic emission and bremsstrahlung. The characteristic line intensity considerably exceeds that of bremsstrahlung in the vicinity of 110 eV (11.4 nm), which is typical for light materials. As it should be, a sharp boundary of the continuous spectrum at the maximum electron energy (5.0 keV in our case) is

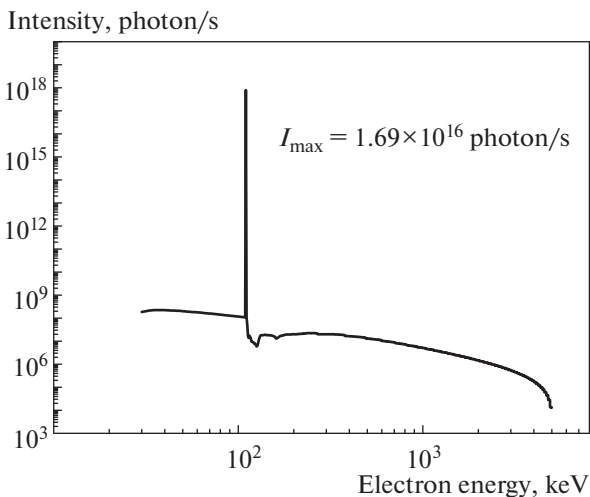


Fig. 3. Emission spectrum of a beryllium target calculated for the shooting through geometry. Calculation parameters are: the electron energy $E_e = 1.0$ keV, the electron current is 1.0 A, the angle of incidence $\theta_{in} = 0$, and the film thickness is 200 nm.

observed, and the bremsstrahlung intensity decreases at energies above the characteristic line energy because of the emission self-absorption in the film. All this confirms the validity of the model constructed.

The break of the continuous spectrum below 30 eV is explained by the break of calculations (electrons were monitored in the target down to the energy 30 eV). Electrons with energies below 110 eV cannot excite the characteristic Br K_α line. However, to observe a change in the bremsstrahlung intensity before and after the characteristic line, electrons with energies from 110 to 30 eV were also studied.

At the first stage, thin film beryllium targets 100, 200, and 400 nm in thickness were simulated in the shooting through geometry. Figure 4 shows the dependences of the conversion coefficient and the absolute intensity of the 11.4-nm characteristic Be K_α line within 4π steradian on the energy of incident electrons.

One can see from the figures presented above that the film with the smaller thickness (100 nm in our case) provides the higher conversion coefficient. The sharp decrease in the radiation intensity and conversion coefficient (the break of plots) at electron energies 4, 5, and 8 keV for 100, 200, and 400 nm thick films, respectively, is caused by the onset of propagation of electrons through the target. This reduces the energy transfer to the target and, thereby reducing the intensity of the 11.4 nm line emitted from the target.

Numerical experiments were performed for determining the optimal film thickness for each acceleration voltage used (0.5–10.0 keV). The optimal thickness was defined as the film thickness providing the maximum absolute intensity of the 11.4-nm Be K_α line

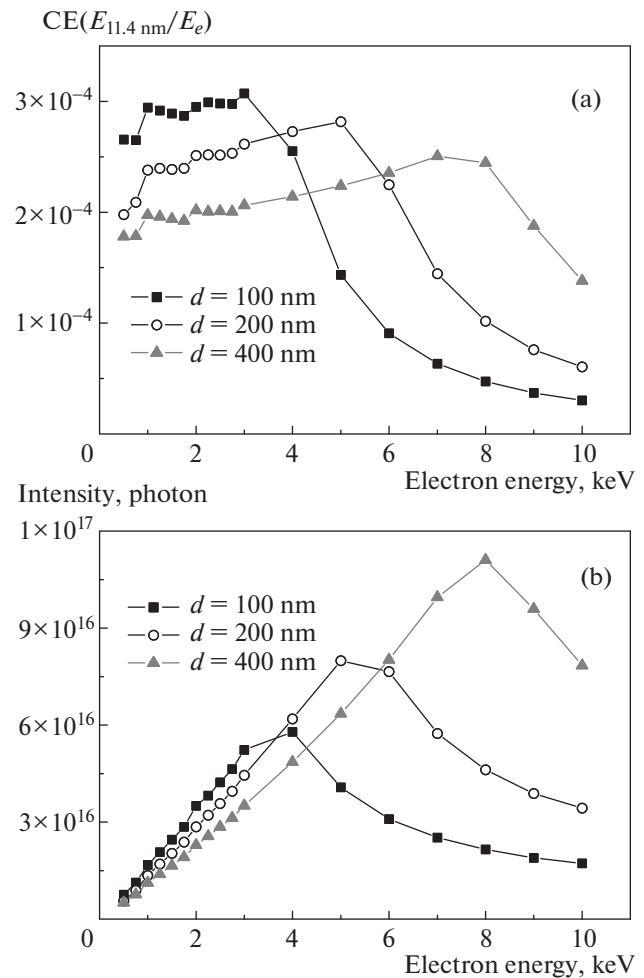


Fig. 4. Dependences of the conversion coefficient of the electron energy to the energy of the characteristic Be K_α line (a) and the absolute intensity of the characteristic K_α line (b) in 4π steradian on the incident electron energy.

emitted within 4π radian in the shooting through geometry and, correspondingly, the maximum conversion coefficient for the given accelerating voltage. The dependence of the conversion coefficient on the film thickness can be qualitatively explained by the following reasons. When the film thickness is small, electrons incident on the target pass through it, not giving all their energy to target atoms. In the case of thick films, electrons lose their energy far from the surface of the shoot through target and radiation produced in the target is lost due to self-absorption in the target. Thus, there exists the optimal thickness providing a compromise between the opposite actions of these effects.

Figure 5 presents the absolute radiation intensity spectra of the Be target, including the K_α line, for the electron energy $E_e = 5.0$ keV and three film thicknesses. The highest radiation intensity corresponds to the 200 nm thick film. One can see that self-absorp-

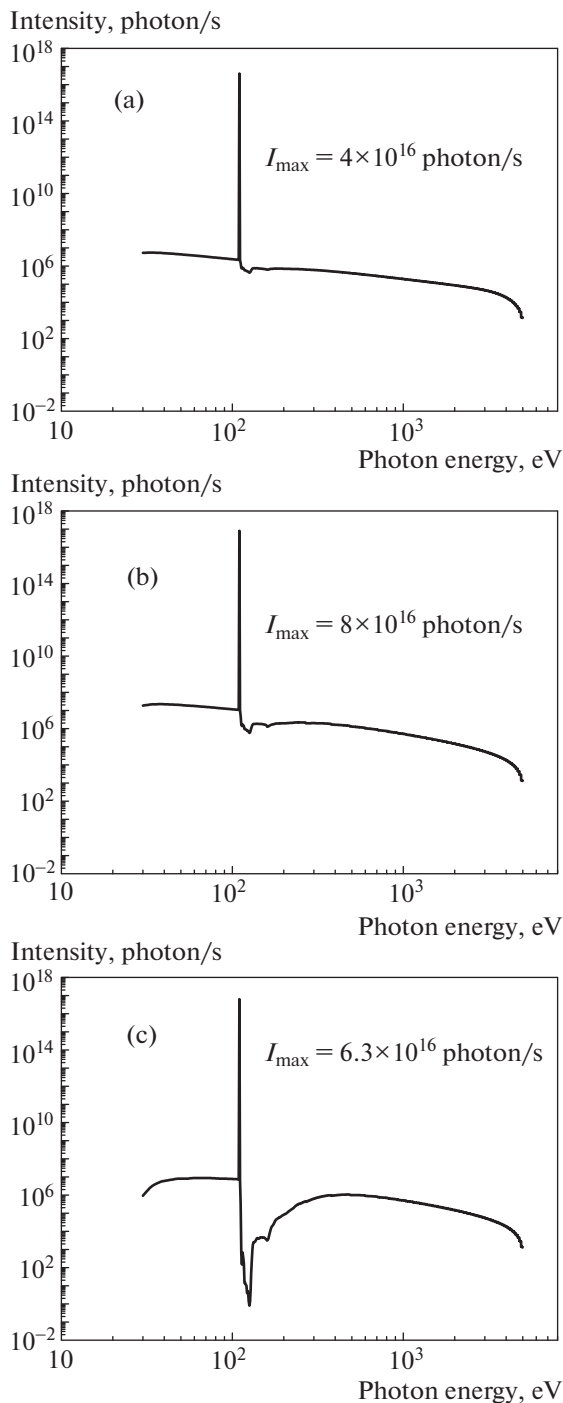


Fig. 5. Absolute emission spectra of the Be target for the electron energy $E_e = 5.0$ keV, electron current 1.0 A and different film thicknesses: (100) (a), 200 (b), and 400 (c) nm.

tion increases with increasing the film thickness (a decrease in the radiation intensity is observed behind the absorption K edge).

Thus, we calculated the optimal film thickness for each accelerating voltage used (0.5–10 keV). Figure 6 presents the dependence of the optimal film thickness on the accelerating voltage.

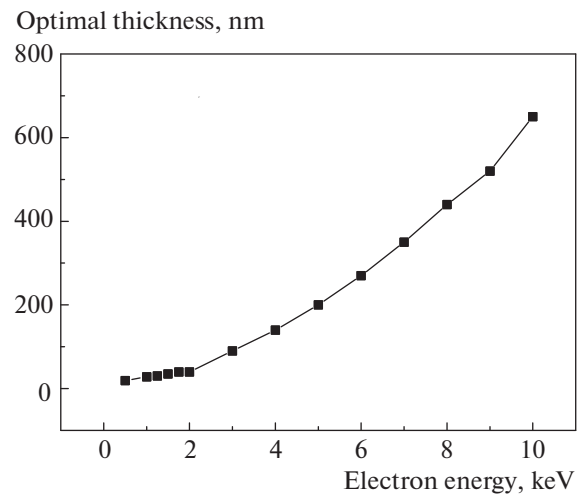


Fig. 6. Dependence of the optimal Be film thickness on the electron energy.

The peak absolute intensities of the $\text{Be}K_\alpha$ line and the conversion coefficients of the electron energy to the $\text{Be}K_\alpha$ line within 4π steradian in the shooting geometry corresponding to these optimal film thicknesses are presented in Fig. 7.

Figure 7 demonstrates a plateau in the dependence of the conversion coefficient on the electron energy in the energy range between 1 and 3 keV, in accordance with the theory [10] predicting that the optimal radiation is achieved for the electron energy about ten ionization potentials.

The maximum conversion coefficient obtained in calculations was 3.0×10^{-4} at the electron energy $E_e = 2.0$ keV for a 40 nm thick freely suspended beryllium film.

3. EXPERIMENTAL RESULTS

A stand on which experiments were performed and an electron gun providing the minimal contamination of a target are described in [20]. As targets, we used freely suspended Be films with different thicknesses prepared by the method described in [21]. The scheme of the experiment is presented in Fig. 8. Electrons emitted by thermocathode 1 and pulled out by accelerating electrode 2 are focused by electromagnetic lens 3 on thin Be film target 4. The target was grounded via a current measuring resistor. For each accelerating voltage, its own value of current through a solenoid was selected. The electron beam incident on the target generates X-rays, which are recorded with a FDUK-100UV absolutely calibrated silicon photodiode with the spectral sensitivity presented in [22].

Parasitic long-wavelength radiation is suppressed by a thin-film absorption filter mounted on the entrance window of the detector. The filter is made of

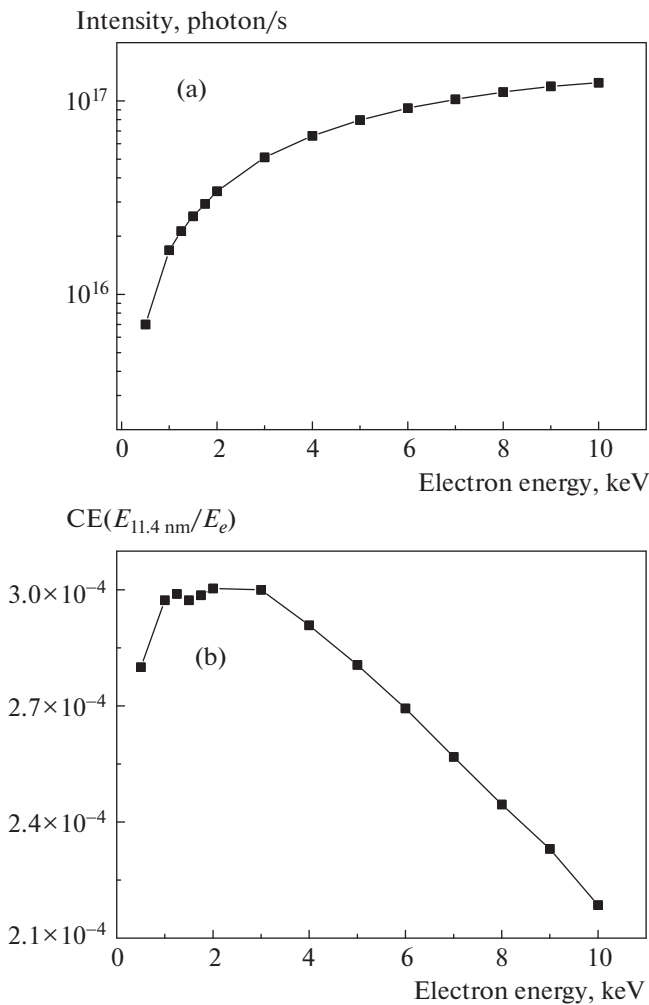


Fig. 7. Peak intensity of the Be K_{α} line (a) and the conversion coefficient of the electron energy to the energy of the characteristic Be K_{α} line (b) in 4π steradian in the shooting through geometry as functions of the electron energy.

a thin (200 nm thick) beryllium film with the transmission spectrum presented in Fig. 9.

One can see that transmission at the working wavelength is about 80%, while the wavelength radiation is suppressed by more than five orders of magnitude ($T_{633 \text{ nm}} = 5.6 \times 10^{-6}$). Because Be has only one characteristic line and the bremsstrahlung intensity is a few orders of magnitude lower than the characteristic radiation intensity, the spectral purity of measurements was fulfilled in the first approximation.

We detected in experiments the dependence of a signal from a target on the accelerating voltage by measuring the electron current on the target. Measurements were performed for shooting through targets 200 and 400 nm in thickness. Figure 10 shows the photograph of the thin 200 nm thick Be film target obtained after experiment.

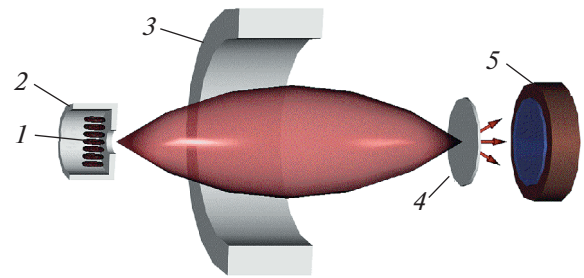


Fig. 8. Scheme of the experiment: (1) thermocathode; (2) accelerating electrode; (3) electromagnetic lens; (4) shooting through target (beryllium film); (5) FDUK-100UB silicon photodiode detector with a thin film filter.

The photograph demonstrates a distinct $2 \times 2 \text{ mm}^2$ imprint of the electron beam. The electron current incident on the beryllium target and the power density corresponding to this current are presented in Fig. 11 as functions of the accelerating voltage.

One can see that the power density on the target noticeably exceeded 1.5 W/cm^2 , corresponding to temperatures no less than 700°C . Note that the film withstood prolonged X-ray exposures. This suggests that a beryllium film can be readily used as a shooting through target from the point of view of thermal loads because the working temperature of the target in a chip of micro focus tubes, which can be manufactured, will not exceed 200°C . The cooling of the target at much higher heat release densities (up to 1 kW/cm^2) will be performed by the heat removal through the chip to an active cooling system.

The dependences of the detector signal on the accelerating voltage for the shooting through beryllium target are presented in Fig. 12.

Beginning from some accelerating voltage, a sharp increase in the signal is observed: for a 200 nm thick film, at the electron energy 3.0–3.5 keV, and for a 400 nm thick film, at the electron energy 4.0 keV. We explain this by a drastic increase in the fraction of electrons propagated through a thin film target and generating radiation from a material located in front of the photodiode of the beryllium filter. This is confirmed by the curves presented in Fig. 13.

For the 200 nm thick film, the propagated electrons appear at the electron energy 2.5 keV, and for the 400 nm thick film, at the electron energy 4.0 keV, which is manifested in a sharp bending of the plot of the dependence of the detector signal on the X-ray tube accelerating voltage.

Then, the conversion coefficient was calculated for the electron beam energy converted to the characteristic Be K_{α} line within the 2π solid angle by the expression

$$CE_{2\pi} = \frac{P_{\text{ph}}}{P_e} \frac{2\pi}{\Omega_d}, \quad (10)$$

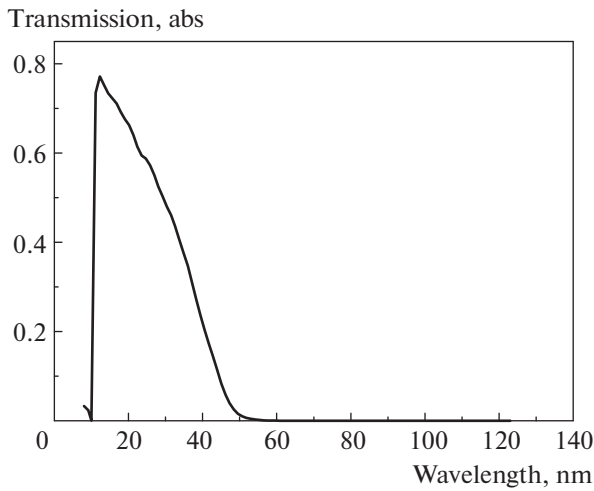


Fig. 9. Transmission spectrum of a thin film 200 nm thick absorption Be filter [23].

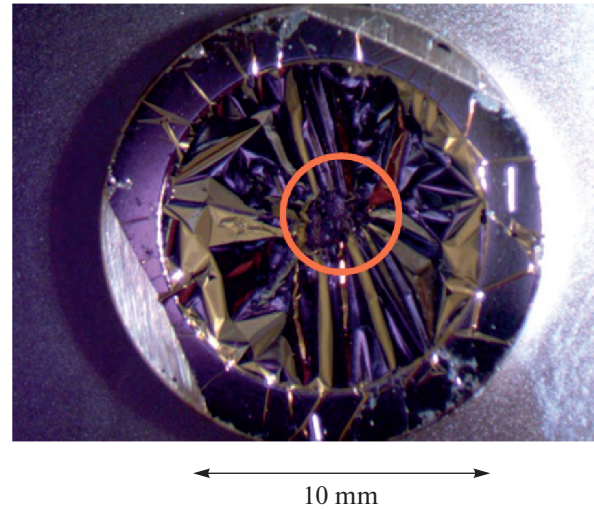


Fig. 10. Photograph of a thin film shooting through target (200 nm thick beryllium film).

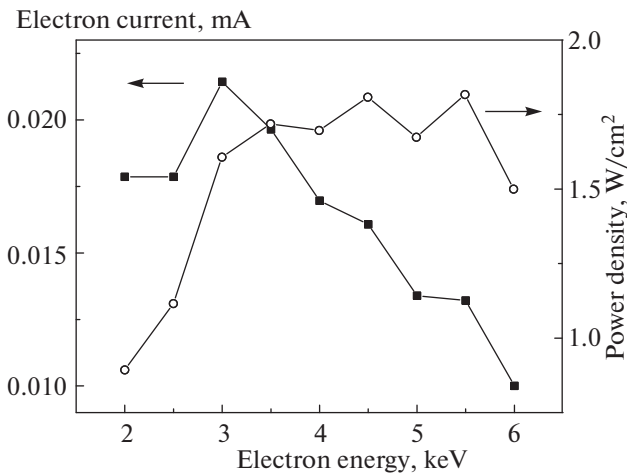


Fig. 11. Electron current on a target and the corresponding power density as functions of the electron density.

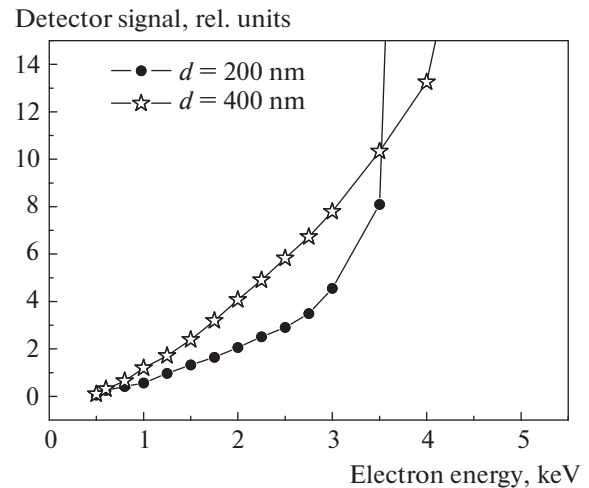


Fig. 12. Dependences of the detector signal on the accelerating voltage.

where P_{ph} is the power of photons emitted from the target into the detector solid angle $\Omega_d = 2.6 \times 10^{-3}$ sr and P_e is the electron beam power.

The power of photons emitted from the target within the solid angle Ω_d is equal to the detected radiation power divided by the spectral filter transmission T_f at the working wavelength 11.4 nm and can be written as

$$P_{ph} = \frac{I_d}{S_d T_f}, \tag{11}$$

where I_d [A] is the detector current, $S_d/[\lambda = 11.4 \text{ nm}] = 0.229 \text{ A/W}$ is the detector sensitivity at the working wavelength [22].

Note that the estimate of the conversion coefficient obtained above is valid only for radiation detection angles close to normal.

The dependence of the conversion coefficient of the X-ray tube electron energy to the characteristic Be K_α line within the 2π solid angle on the electron energy is presented in Fig. 14.

The maximum value of the conversion coefficient measured within the 2π solid angle was 4.6×10^{-5} for the 200-nm thick film and the electron energy 2.75 keV. This corresponds to the conversion coefficient within the 4π solid angle about 9.2×10^{-5} , which is approximately three times smaller than the calculated value. Thus, the contribution of inelastic scattering to the total interaction cross section proved to be overstated in our model, because we used ionization

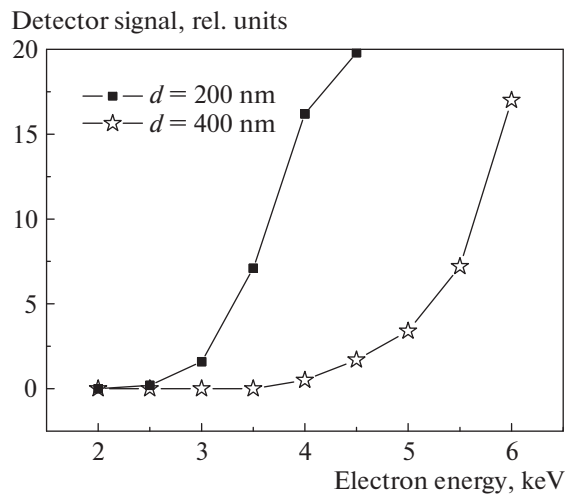


Fig. 13. Current of propagated electrons as a function of the electron energy (accelerating X-ray tube voltage for 200 and 400 nm thick films).

cross sections from [13]. These cross sections are noticeably closer to experimental results than these obtained in [9], but also differ from experimental values. Therefore, to refine the calculation method, it is necessary to correct interaction cross sections. The study of the spectrum of propagated electrons and the measurement of the conversion coefficient directly in the transmission band of a lithograph require separate considerations.

4. CONCLUSIONS

Software for Monte Carlo simulations of the interaction of accelerated electrons with a thin film shooting through target has been written. The program was used for calculating the absolute radiation intensity of a beryllium target depending on the film thickness and the accelerating electron energy. The maximum calculated conversion coefficient of the electron energy to the energy of the characteristic $\text{Be}K_\alpha$ line within 4π steradian in the shooting through geometry was $\text{CE} = 3.0 \times 10^{-4}$ for the electron energy $E_e = 2.0$ keV and a 40 nm thick freely suspended beryllium film.

Practically important results of the work are experimentally measured conversion coefficients of the electron beam energy to the characteristic $\text{Be}K_\alpha$ line in the electron energy range 0.5–3 keV for 200 nm and 400 nm thick films. The maximum value of the measured conversion coefficient recalculated to 4π steradian was $\text{CE} = 9.2 \times 10^{-5}$ for the 200 nm thick film and the electron energy $E_e = 2.75$ keV. In addition, an important result was the demonstration of a prolonged operation of a submicron beryllium film as an anode of an X-ray tube. The typical thermal loads on film samples exceeded 1.5 W/cm^2 during measurements, corresponding to the heating of the central region of

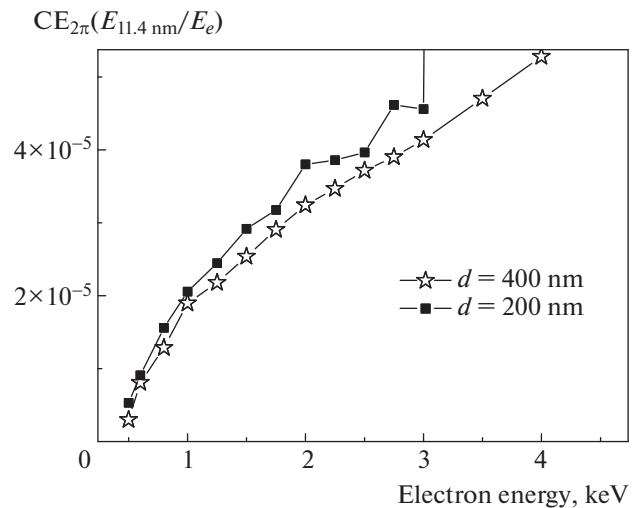


Fig. 14. Dependences of the conversion coefficient of the electron energy to the energy of the characteristic $\text{Be}K_\alpha$ line to the solid angle 2π for an X-ray tube with shooting through targets made of freely suspended 200 and 400 nm thick beryllium films.

films up to temperatures above 700°C , however, without their break or rapid degradation of their characteristics.

Experimental data on the conversion efficiency of the electron beam energy to the soft X-ray energy in shooting through beryllium targets suggest the necessity of correcting Be ionization cross sections presented in the literature.

ACKNOWLEDGMENTS

The work was performed using the equipment of “Microsystem technique and electronic component base,” MIET and was supported by the Ministry of Education and Science of the Russian Federation, Agreement no. 14.578.21.0250 (RFMEF15781X0250).

REFERENCES

1. N. A. Dyuzhev et al., *Kratk. Soobshch. Fiz. FIAN*, No. 12, 56 (2017).
2. A. Basu et al., *J. Phys. D: Appl. Phys.* **48**, 225501 (2015).
3. N. I. Chkhalo and N. N. Salashchenko, *AIP Adv.* **3**, 082130 (2013).
4. C. Montcalm et al., *Proc. SPIE* **3331**, 42 (1998).
5. M. O. Krause, *J. Phys. Chem. Ref. Data* **8**, 307 (1979).
6. www.evex.com.
7. <http://microanalyst.mikroanalytik.de/software.phtml>.
8. <http://montecarlo modeling.mcgill.ca/>.
9. E. Casnati, *J. Phys. B: At. Mol. Phys.* **15**, 155 (1982).
10. M. A. Blokhin, *The Physics of X-Rays* (GITTL, Moscow, 1953; United States Atomic Energy Commission, Office of Technical Information, 1961), rus. p. 87.

11. <http://xdb.lbl.gov/>.
12. V. P. Afonin and V. I. Lebed', *Monte-Carlo Method in X-ray Spectral Analysis* (Nauka, Novosibirsk, 1989), p. 6 [in Russian].
13. T. Maihom, *Eur. Phys. J. D* **67**, 2 (2013).
14. A. A. Abrahamson, *Phys. Rev.* **178**, 76 (1969).
15. H. Bethe, *Ann. Phys. (Leipzig)* **5**, 325 (1930).
16. F. Bloch, *Z. Phys. A* **22**, 363 (1993).
17. Y.-K. Kim, *Phys. Rev. A* **65**, 022705 (2002).
18. M. A. Blokhin and I. G. Shveitser, *X-Ray Spectral Handbook* (Nauka, Moscow, 1982), p. 38 [in Russian].
19. http://www-cxro.lbl.gov/optical_constants/pert_form.html.
20. M. S. Bibishkin et al., *Proc. SPIE* **5401**, 8 (2004).
21. N. I. Chkhalo et al., *Appl. Opt.* **55**, 4683 (2016).
22. P. N. Aruev, M. M. Barysheva, B. Ya. Ber, N. V. Zabrodsкая, V. V. Zabrodskiy, A. Ya. Lopatin, A. E. Pestov, M. V. Petrenko, V. N. Polkovnikov, N. N. Salashchenko, V. L. Sukhanov, and N. I. Chkhalo, *Quantum Electron.* **42**, 943 (2012).
23. http://henke.lbl.gov/optical_constants/.

Translated by M. Sapozhnikov

SPELL: OK

SPELL: 1. steradian